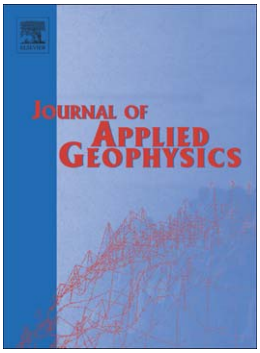

A case study on swell correction of Chirp sub-bottom profiler (SBP) data using multi-beam echo sounder (MBES) data

Young-Jun Kim, Nam-Hyung Koo, Michael Riedel, Hyun Namgoong, Jeong-Min Lee, Snons Cheong, Yonghwan Joo, Dong-Geun Yoo, Jong-Hwa Chun, Ho-Young Lee

PII: S0926-9851(17)30251-3
DOI: doi:10.1016/j.jappgeo.2017.08.001
Reference: APPGEO 3317

To appear in: *Journal of Applied Geophysics*

Received date: 13 March 2017
Revised date: 8 June 2017
Accepted date: 3 August 2017

Please cite this article as: Kim, Young-Jun, Koo, Nam-Hyung, Riedel, Michael, Namgoong, Hyun, Lee, Jeong-Min, Cheong, Snons, Joo, Yonghwan, Yoo, Dong-Geun, Chun, Jong-Hwa, Lee, Ho-Young, A case study on swell correction of Chirp sub-bottom profiler (SBP) data using multi-beam echo sounder (MBES) data, *Journal of Applied Geophysics* (2017), doi:10.1016/j.jappgeo.2017.08.001

A case study on swell correction of Chirp sub-bottom profiler (SBP) data using multi-beam echo sounder (MBES) data

Young-Jun Kim[a*], Nam-Hyung Koo[a,b], Michael Riedel[c], Hyun Namgoong[d], Jeong-Min Lee[d], Snons Cheong[e], Yonghwan Joo[a], Dong-Geun Yoo[a], Jong-Hwa Chun[a], Ho-Young Lee[a]

[a] Petroleum and Marine Research Div., Korea Institute of Geoscience and Mineral Resources (KIGAM), 124, Gwahak-ro, Yuseong-gu, Daejeon 34132, Republic of Korea

[b] Department of Petroleum Resources Technology, University of Science and Technology (UST), 217 Gajeong-ro, Yuseoung-gu, Daejeon 34113, Republic of Korea

[c] GEOMAR Helmholtz Centre for Ocean Research, Wischhofstr. 1-3, 24148 Kiel, Germany

[d] Korea Seabed Information Co., Gyeryong-ro 394, Seo-gu, Daejeon 35270, Republic of Korea

[e] Climate Change Mitigation and Sustainability Div. Korea Institute of Geoscience and Mineral Resources (KIGAM), 124, Gwahak-ro, Yuseong-gu, Daejeon 34132, Republic of Korea

* Corresponding author. Tel: +82 42 868 3190; Fax: +82 42 868 3417

E-mail address: kimyj@kigam.re.kr (Y.-J. Kim).

ABSTRACT

High-resolution marine seismic data acquisition and subsequent analyses are highly influenced by sea conditions, directly affecting data quality and interpretation. Traditional swell effect correction methods are effective in improving reflector continuity; however, they are less useful for enhancing travel time consistency at intersection points of crossing lines. To develop a robust swell-removal technique for a set of crossing lines multi-beam echo sounder (MBES) data and Chirp sub-bottom profiler (SBP) data were acquired. After generation of a time structure map of the sea-bottom converted from the final processed multi-beam data, a moving average was used to improve the event continuity of the sea-bottom reflection of the Chirp SBP data. Using the position of the Chirp SBP data, the difference between the travel time of the sea-bottom from the smoothed map and the original travel time of the sea-bottom is calculated as a static correction. The static correction method based on the MBES data was compared and verified using three different cases: (i) simple 2D swell effect correction on a line-by-line basis, (ii) comparing the swell corrections at the crossing positions of 2D lines acquired from different dates, and (iii) comparison of ties of intersection points between 2D lines after new swell correction applied. Although a simple 2D swell correction showed great enhancement of reflector continuity, only the full static correction using the newly proposed method using MBES data produced completely corrected reflection events especially at the crossing points of 2D lines.

Keywords: Chirp sub-bottom profiler, Multi-beam echo sounder, Marine high-resolution, Swell effect, Static correction, Mis-tie correction

1. Introduction

Sea state during acquisition strongly influences quality of high-resolution marine seismic data. In case of a conventional seismic survey for oil and gas, the target depth is much deeper and vertical resolution of the dataset is lower, since the seismic source is typically an air-gun (or array of guns) with dominant frequencies between 40 Hz to 70 Hz. Additionally, to avoid swell and wave effects, the streamer is towed at a considerable depth below sea level (Lee et al., 2013). In contrast, high-resolution marine seismic data acquired by Chirp sub-bottom profiler (SBP) with dense ping interval acquisition parameters are strongly influenced by swell, and swell causes a significant decline of the horizontal resolution. By using a wide bandwidth of the signal, Chirp SBP achieves optimum penetration and good resolution. The signal-to-noise ratio (SNR) is improved by correlating the acquired reflection data with the full waveform of the source signature (Baradello, 2014; Gutowski et al., 2002). Chirp SBP systems have been applied in a variety of marine geological and geophysical fields, such as mapping, geohazard, geo-technical and archaeological studies (Bull et al., 2005; Gutowski et al., 2002; Kim et al., 2016). Chirp SBP data with dominant frequencies between 2 kHz and 7 kHz provide decimeter vertical resolution (Gutowski et al., 2002; Quinn et al., 1997; Schock et al., 1989), much finer than the typical sea state during marine seismic data acquisition. If the height of the swell is higher than the vertical resolution, this swell can have detrimental effects on data quality of Chirp SBP data (Lee et al., 2002). The continuity of the seismic reflection events related to the sub-bottom structures is strongly reduced and it may be impossible to distinguish swell-effects from real geological phenomena, such as fault offsets. Thus, improper (or no) swell correction can lead to erroneous interpretations.

In less than 200 m water depth, the ping interval of a typical Chirp SBP survey is set to less than 1.0 s. With a survey vessel speed of 4.5 knots, high-resolution seismic data with dense horizontal resolution at ~2.3 m are obtained. Assuming for example a swell height of 1.5 m, the two-way travel time of reflections is moved up and down by about 1.0 ms (seawater velocity = 1,500 m/s) every wave cycle. Additionally, source and receiver (if physically de-coupled) can move independently from each other

and produce a complex composite swell effect on the data.

Swell effect corrections are divided into two steps, consisting of sea-bottom detection and subsequent swell suppression. In order to effectively remove the swell, accurate sea-bottom detection on the seismic dataset is important (Lee et al., 2015). One method of sea-bottom detection is based on the cross-correlation scheme, which recognizes the sea-bottom at the point of maximum cross-correlation between the seismic source signal and the reflected signal trace (Kim et al., 2003). A second method utilizes the reflection amplitude of the sea-bottom. This method is in principle the image color sampling method used for color classification of seismic sections (Kim and Kim, 2004). Swell effect suppressions can be implemented by a moving average method and high-cut filtering methods using the sea-bottom travel time of adjacent traces as control points. Lee et al. (2002) compared the corrected seismic sections produced by these two methods, which showed comparable outcomes. However, since excessive swell effect correction can sometimes produce artificial distortion of the actual sea-bottom and lower sedimentary layers, one has to consider adjacent traces of crossing lines and general seafloor topography to achieve a geologically meaningful interpretation of the data.

To develop a robust swell correction, we use multi-beam echo sounder (MBES) data as reference to define a static correction that removes the swell while maintaining proper geological structures. MBES systems typically have a large number of transducers, each operating over a narrow beam angle (0.5° – 1.5°) and thus can cover a distance both sides along a survey ship's track which is about equal to twice the water depth. Since MBES systems can acquire dense bathymetry data, these surveys provide 100 % coverage of the seafloor (Pandian et al., 2009). MBES systems use sources with dominant frequencies of several 10s of kHz and MBES data are acquired to generate high-resolution bathymetric maps and to provide e.g. means for sea-bottom sediment classification across the survey area (Pandian et al., 2009; Pratson and Edwards 1996). The MBES survey also provides the most reliable water depth even during considerable swell conditions. During acquisition, the MBES data are corrected using observed values

of the gyro compass and the motion sensors of the vessel. The sound velocity profile within the survey area and the sea-surface sound velocity are measured to accurately convert travel time to water depth. The final bathymetric map is considered as reference for the spatial continuity of the seafloor reflection. For the purpose of this study, we simultaneously acquired Chirp SBP data and MBES data.

In order to develop a robust algorithm and to optimize incoherent travel times for the same reflection events on the same line locations, the survey was conducted at two consecutive days. To verify the new swell correction proposed, we compare the Chirp SBP sections produced by a traditional moving average method with the new algorithm.

2. Survey Method

The survey was conducted using the R/V Tamhae II owned by the Korea Institute of Geoscience and Mineral Resources (KIGAM). The Chirp SBP system consisted of the hull-mounted 16 transducers and a Bathy 2010 SyQwest recording system. The MBES system was also hull-mounted and acquisition was performed using the Kongsberg EM 302 system. The water depth of our survey area ranged from 110 to 135 m, and the ping interval of the Chirp SBP acquisition was set to 1 second. The speed ranged from 4.31 to 5.64 knots and the distance between adjacent pings ranged from 2.22 to 2.90 m, respectively. The ping interval of MBES data acquisition is defined automatically by the EM302 system, and depends on water depth. All detailed data acquisition parameters are summarized in Table 1. To measure sound velocity in our study region, we used one expendable bathythermograph (XBT), launched from the survey vessel prior to the acquisition of all Chirp SBP and MBES data.

The survey area is located off Pohang in the East Sea, Korea (Figure 1). This survey was composed of 5 track lines which were about 1 km long. The survey consists of two lines in a south-north direction, two lines in east-west direction, and one line in southwest-northeast direction. In order to maximize any swell effect on the Chirp SBP data, the survey was conducted under severe weather conditions and swell

reached a maximum wave height of 3.0 m. To verify a possible travel time gap of the seafloor (and sub-seafloor reflections) along the same line-positions, we twice performed the surveys for Chirp SBP line 101 and 104. The primary survey and the secondary survey are represented by blue and red lines, respectively in Figure 1. Chirp SBP line 106 was designed to create as many intersection points as possible as shown in Figure 1.

3. Multi-beam Echo Sounder Data

In the first step of our proposed algorithm, the MBES bathymetric data were converted to two-way travel time (in seconds) below sea surface using the average sound velocity profile acquired in the region of the study area (Figure 2). After the geographic ping position was defined for the Chirp SBP data, the corresponding sea-bottom reflection time values of each ping were extracted from the converted bathymetric map. The differences between the extracted and the detected values of the seafloor reflection in the Chirp SBP data are then calculated.

Figure 3 shows the process of conversion from water depth to two-way travel time on the bathymetric map of the study area. The processing of the MBES data contained the correction of navigation data using the measured sound velocity, tidal correction, and removal of mis-measured peak values every survey line. Figure 3(a) is the bathymetric map produced by the final processed MBES data. (Figure 3a). Figure 3b shows the sound velocity profile, obtained using an XBT used for the processing of MBES data. Figure 3c is the converted bathymetric map in time (units of milliseconds) applying a velocity of 1481.2m/s, as represented in Figure 3b.

4. Static Correction using the Multi-beam Echo Sounder Data

4.1. Swell Effect Correction

The sea-bottom was detected as the first largest trough amplitude on the Chirp SBP data and manually picked trace-by-trace. In order to improve the reflection event continuity on the Chirp SBP sections, the seafloor topography was smoothed using a moving average as shown in Figure 4. The size of the cell of the moving average was set to 14.5 m × 14. 5 m. Thus, a cell could include 5 or 6 traces depending on the survey vessel speed. Figure 4a is identical to Figure 3c with a grid cell-size of 1 × 1 (14.5 ×14.5 m) for the moving average window and shows an irregular surface. The sizes of the other grids used were 3 × 3 (43.5 × 43.5 m), 5 × 5 (72.5 × 72.5 m) and 7 × 7 (101.5 × 101.5 m) (Figures 4b, 4c and 4d). As the grid sizes increase, the time structure map becomes gradually smoother. The smoothing operator cutoff was determined based on visual inspection of the time structure maps. The raw data (Figure 4a) are dominated by a high-frequency noise with typical spatial dimensions of 30 m to 40 m length (Figure 3c). These small stripes are oriented at ~ 45 degrees from North. Removing these artifacts requires an operator length of minimum 3 × 3 cells (43.5 × 43.5 m). However, as seen in Figure 4b, this smoothing operator length is insufficient to fully remove this linear noise. Instead, using the 5 × 5 cells operator length improves the image sufficiently well to remove the linear noise (Figure 4c). Higher smoothing cell-sizes (e.g. Figure 4d) add no further improvement.

Figure 5 shows the sections of Chirp SBP line 101 (indicated by a green thick line in Figure 1) before and after the swell effect correction. A typical example of uncorrected data is given in Figure 5a, before the swell effect correction was applied. A very rough sea-bottom reflection is seen with the travel time of reflection moving up and down with a cycle between 5 and 7 sec. A clear sedimentary layer is observed underneath the sea-bottom, and its surface also shows the same rough topography due to the swell.

By applying a seventeen-point moving average, improved reflector-continuity of the sea-bottom an underlying sediment layer can be confirmed (Figure 5b). The two-way travel time depth of the sea-bottom at ping number 301 along line 101 is ~160 ms and gradually deepens toward the east. Figure 5c shows the same section of line 101 with the new static correction method applied based on the time

bathymetric map (Figure 4a) generated by a moving average of a grid size of 1 × 1. Some swell effect remains on the section overall. A difference in the travel time of the sea-bottom of approximately 8.0 ms between sections shown in Figures 5b and 5c is caused by the conversion from water depth to travel time using an average sound velocity. Gradually increasing the smoothing grid cell-size of the bathymetry from 3 × 3 (Figure 5d) to 5 × 5, and 7 × 7 (Figures 5e and 5f) demonstrates the smoothing and removal of swell from the Chirp SBP data. We chose a grid size of 5 × 5 for our final swell-removal algorithm, considering that any additional smoothing may introduce artificial or excessive smoothness. Also, no further improvement in swell removal was seen given the vertical resolution given by the sample rate of the SBP data.

4.2. Static Correction at crossing points of lines

The travel time of reflection events changes according to the survey direction and time of acquisition. Figure 6 shows the sections of Chirp SBP lines 104 and 104A as well as graphs comparing the travel time of sea-bottom before and after the swell effect correction. The survey progress direction of line 104 and 104A are the same (180 degrees direction) but the days of data acquisition are different. The interval of ping number from 1 to 500 of Chirp SBP line 104 corresponds to the interval of ping number from 25 to 450 of Chirp SBP line 104A. This corresponding interval is indicated by a green dotted rectangle in Figure 1. Figures 6a and 6b show the sections of Chirp SBP line 104 and 104A before the swell effect correction, respectively. The sea-bottom and the sediment layer underneath are heavily distorted by swell.

Figure 6c depicts the travel time of the sea-bottom of the two lines shown in Figures 6a and 6b, as function of the Y-coordinate (UTM North) ping positions. The travel time of the sea-bottom reflection along line 104 is generally higher than that of line 104A. Figure 6d and 6e show the sections after the swell effect correction using the moving average and the removal of the swell effect, respectively. Both

show the same overall topography and similar sub-seafloor layer-morphology. However, as seen in Figure 6f, large discrepancy of the sea-bottom travel time exists. The travel time of sea-bottom of the overlapping intervals between line 104 and line 104A (corresponding parts between 3991350 and 3991650 on the northing values), is entirely different (highlighted by an arrow in the images). This is a result of different weather conditions between the dates of acquisition, especially the height of swell. Figures 6g and 6h show the sections after new static correction using the MBES data was applied. These sections show an improved reflector-continuity (Figures 6d and 6e) and the travel time of sea-bottom at the overlapping intervals exactly match (Figure 6i). Some minor remaining differences between the swell-corrected lines 104 and 104A seen in Figure 6i are due to slightly different geographical locations of the two lines (compare to Figure 1).

4.3. Tie Correction at intersection points

The frequency band of Chirp SBP data used in this study ranges from 2,750 to 6,750 Hz, so that the dominant wavelength is approximately 0.32 m. The shorter the wavelength, the higher the mis-tie occurrence probability on intersection points of individual lines. The survey lines are designed with eight intersection points.

Figure 7 shows a comparison of the data at the intersection points on Chirp SBP sections after the swell correction. Figure 7a is an enlarged track chart (indicated by a green dotted square in Figure 1) and shows the three intersection points formed by three survey lines (Chirp SBP line 102, 103 and 106). The numbers and cycles on the survey lines are indicated by the corresponding ping numbers. The red dotted arrows and the alphabetical order indicate the display sequence of Chirp SBP sections. The Chirp SBP sections after swell correction using the moving average are shown in Figure 7b. We can observe that the continuity of the reflections is improved overall, but at the cross points the data do not match. The travel time differentials between A and B (Figure 7b), between B and C, and between C and D are

about 0.2 ms, 0.3 ms, and 1.5 ms, respectively. The travel time differentials at each intersection points are not identical, thus, this cannot easily be corrected by a bulk shift. In contrast, Figure 7c shows the same data with the new swell correction method applied, using the time bathymetric map produced by a moving average of a grid size of 5 × 5with shows both, enhanced reflector continuity and an exact match of travel time at each intersection point.

5. Conclusions

High-resolution marine seismic data require a suitable static correction method to compensate for swell effect and tidal variations, in accordance with data acquisition conditions. To overcome these various problems, an objective reference frame is required such as the MBES topographic map of seafloor. We acquired Chirp SBP and MBES data simultaneously to develop a new technique for an effective swell correction. Smoothing of the MBES data is performed with an optimal 5 × 5 grid cell size in this study to improve the reflection events continuity on the Chirp SBP sections.

By comparison with the Chirp SBP sections produced by a traditional moving average method on as follows, the new swell correction was able to demonstrate the superiority. The moving average method is useful to remove rough sea-bottom reflectors induced by strong swell, but it creates a mismatch of the sea-bottom travel time for data from different data acquisition dates. Also, the travel time of the ties at intersection points produced by the moving average method is different at each tie-point. In contrast, the newly proposed swell correction produces Chirp SBP sections with an effective swell suppression and an exact match of travel time of data from different data acquisition dates and at all intersection points. Thus, the newly proposed swell correction can be applied for the various static corrections at one time.

Acknowledgements

This research was supported by the Korea Institute of Geoscience and Mineral Resources (KIGAM). We thank all shipboard scientists and crew R/V Tamhae II for their efforts in the field survey. This research was partly supported by the project titled "Studies on Gas Hydrate Resource Assessment and Characterization of Chimney Structures in the Ulleung Basin (16-1141)" and "Development of engineering-scale 3D system for marine seismic exploration (17-3314)".

References

Baradello, L., 2014, An improved processing sequence for uncorrelated Chirp sonar data, Marine Geophysical Researches, 35, 337-344.

Bull, J.M., Gutowski, M., Dix, J.K., Henstock, T.J., Hogarth, P., Leighton, T.G., White, P.R., 2005, Design of a 3D Chirp sub-bottom imaging system, Marine Geophysical Researches, 26, 157-169.

Gutowski, M., Bull, J., Henstock, T., Dix, J., Hogarth, P., Leighton, T., White, P., 2002, Chirp sub-bottom profiler source signature design and field testing, Marine Geophysical Researches, 23, 481-492.

Kim, J.H., Lee, H.Y., Kim, J.S., Kang, D.,H., 2003, Suppression of swell effect in high-resolution marine seismic data using cross-correlation scheme, J. of the Korean Geophysical Society, 6, 31-38.

Kim, J.H., Kim, H.D., 2004, An accurate sea bottom detection by image color reduction method, Publications of Ocean Resources & Research Institute of Dong-A University, 16, 1-6.

Kim,Y.-J., Koo, N.-H., Cheong, S., Kim, J.-K., Chun, J.-H., Shin, S.-R., Riedel, M., Lee. H.-Y., 2016, A case study on pseudo 3-D Chirp sub-bottom profiler (SBP) survey for the detection of a fault trace in shallow sedimentary layers at gas hydrate site in the Ulleung Basin, East Sea, Journal of Applied Geophysics, 133, 98-115.

Lee, H.-Y., Koo, N.-H., Park, K.-P., Kim, J.-K., Kim, W.-S., and Kang, D.-H., 2002, Suppression of swell effect in 35 kHz subbottom profiler data, "The Sea" J. of the Korean Society of Oceanography, 7, 95-99.

Lee, H.-Y., Koo, N.-H., Kim, W., Kim, B.-Y., Cheong, S., Kim, Y.-J., 2013, Swell effect correction for the high-resolution marine seismic data, Jigu-Muli-wa-Mulli-Tamsa, 16, 240-249.

Lee, H.-Y., Koo, N.-H., Kim, W., Kim, B.-Y., Cheong, S., Kim, Y.-J., Son, W., 2015, Swell effect correction of sub-bottom profiler data with weak sea bottom signal, Jigu-Muli-wa-Mulli-Tamsa, 18, 181-196.

Pandian, P.K., Ruscoe, J.P., Shields, M., Side, J.C., Harris, R.E., Kerr, S.A., Bullen, C.R., 2009, Seabed habitat mapping techniques: an overview of the performance of various systems, Mediterranean Marine Science, 10, 29-43.

Pratson, L.F., Edwards, M.H., 1996, Introduction to advances in seafloor mapping using sidescan sonar and multibeam bathymetry data, Marine Geophysical Researches, 18, 601-605.

Quinn, R. Bull, J.M., Dix, J.K., 1998, Optimal processing of marine high-resolution seismic reflection (Chirp) data, Marine Geophysical Researches, 20, 13-20.

Schock, S. G., LeBlanc, L. R., Mayer, L. A., 1989, Chirp subbottom profiler for quantitative sediment analysis, Geophysics, 54, 445-450.

Table List

Table 1. Survey equipment and data acquisition parameters.

Table 1.

Vessel	Tamhae 2	
Survey Method	Chirp SBP	Multi-beam Echo Sounder
GPS	C-Nav DGPS System	Seapath 300 (including the ability of motion sensor)
Acquisition System	Bathy 2010 (SyQwest)	EM302 (Kongsberg)
Number of Transducer / Beam	16	288
Frequency Bands	2.75 – 6.75 kHz	30 kHz
Pulse Length	25 ms	
Ping Interval	1 s	Auto
Resolution	24 bits	
Sampling Interval	0.05 ms	

Figure List

Figure 7. Comparison of the results of the ties at the intersection points formed by Chirp SBP line 102, 103 and 106 after the swell correction in accordance to the application method. (a) The enlarged survey tracks of the cross points. The red dotted arrows and A, B, C and D indicates the display order of Chirp SBP line 102, 103 and 106. (b) The Chirp SBP sections after the swell correction using the moving average. (c) The Chirp SBP sections after the new static correction using the multi-beam echo sounder data which applied the moving average by the grid size of 5 × 5.

Figure 1.

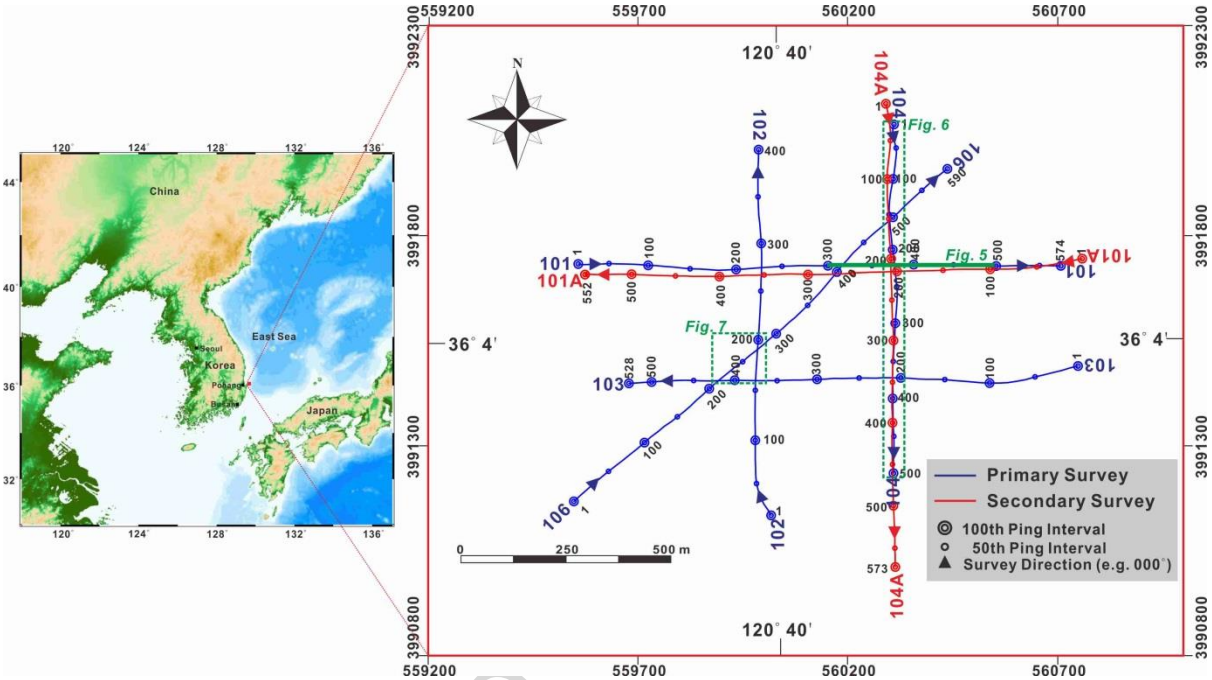

Figure 2.

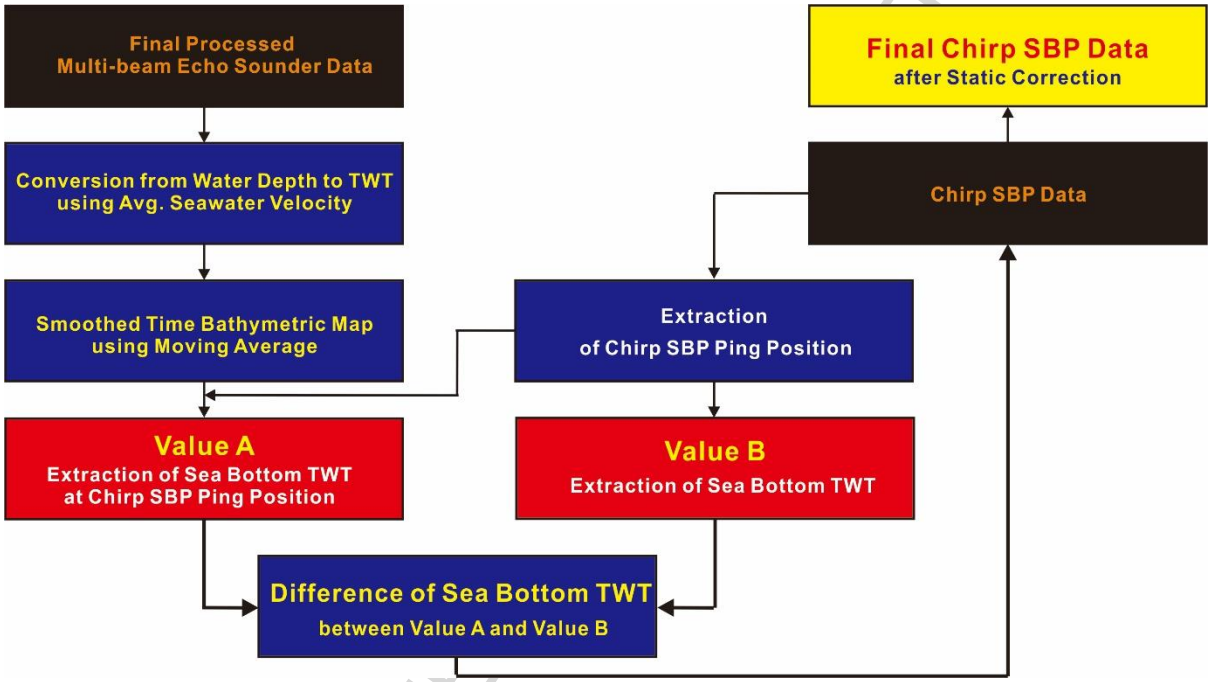

Figure 3.

(a)

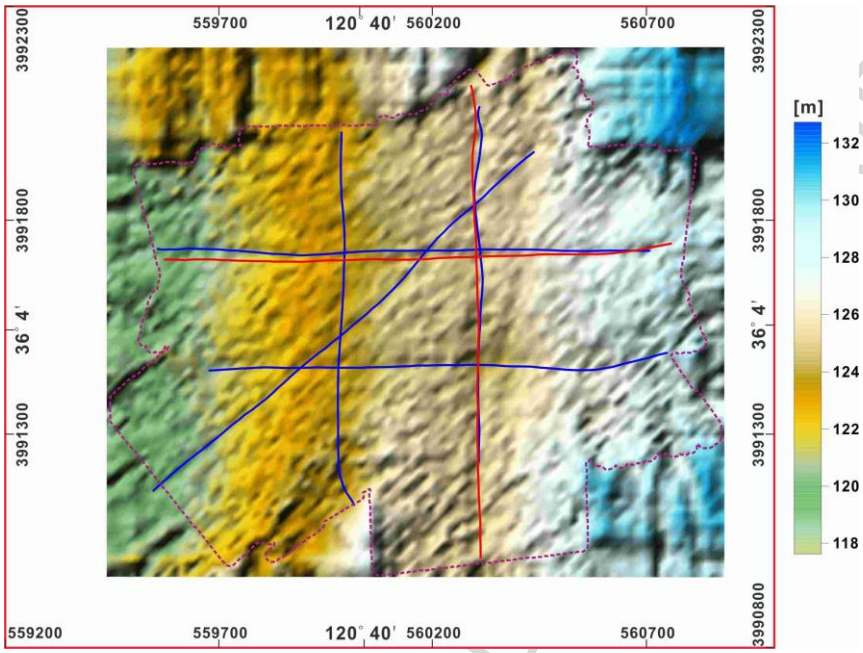

(b)

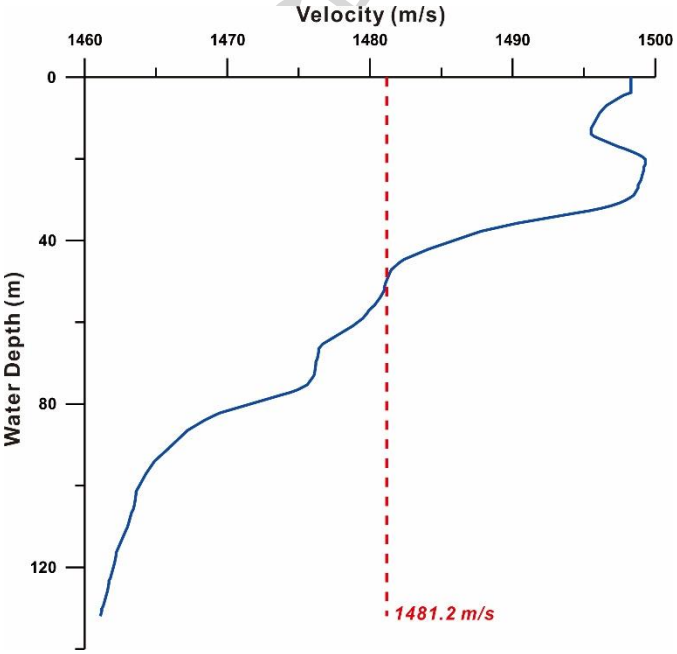

(c)

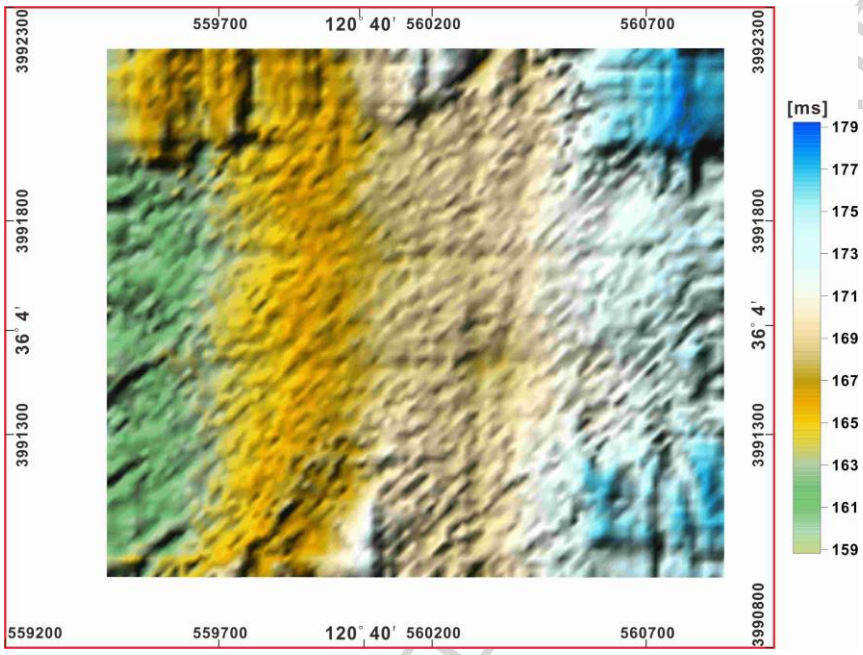

Figure 4.

(a) (b)

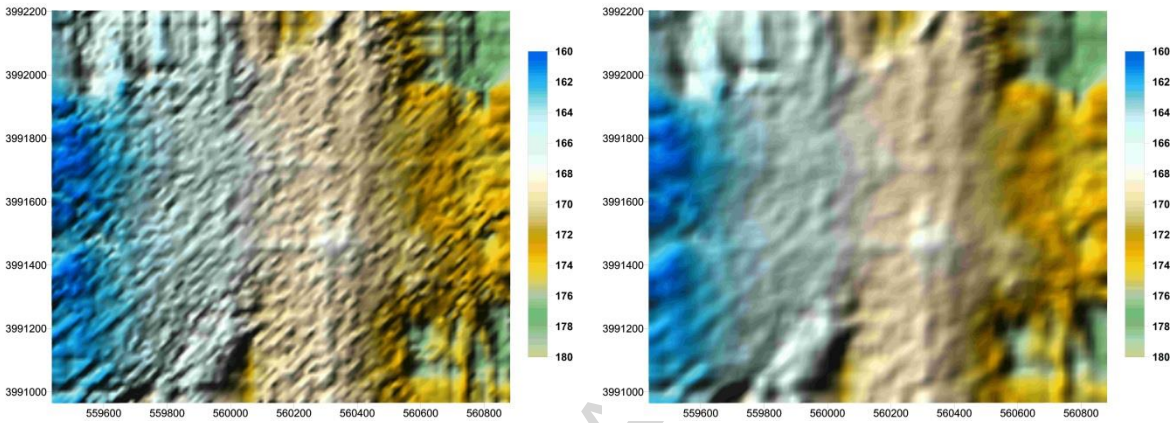

(c) (d)

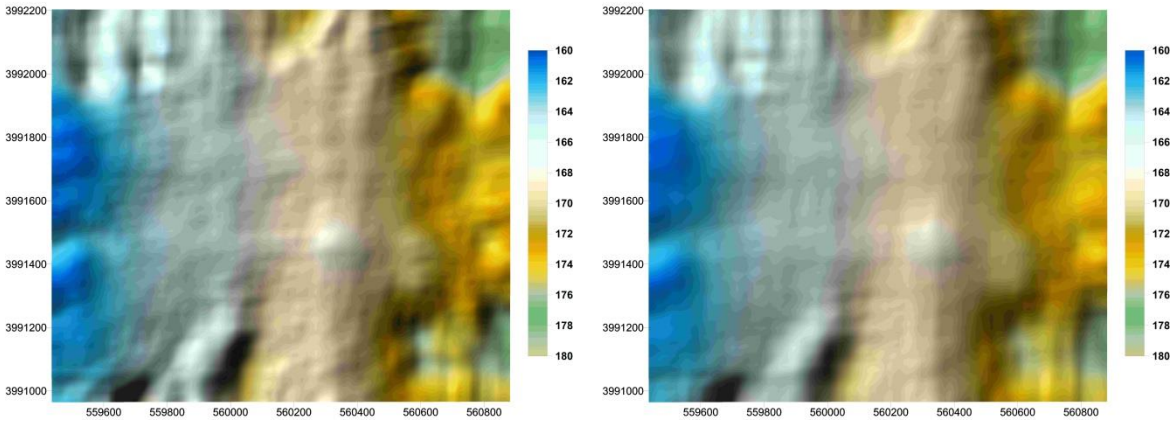

Figure 5.

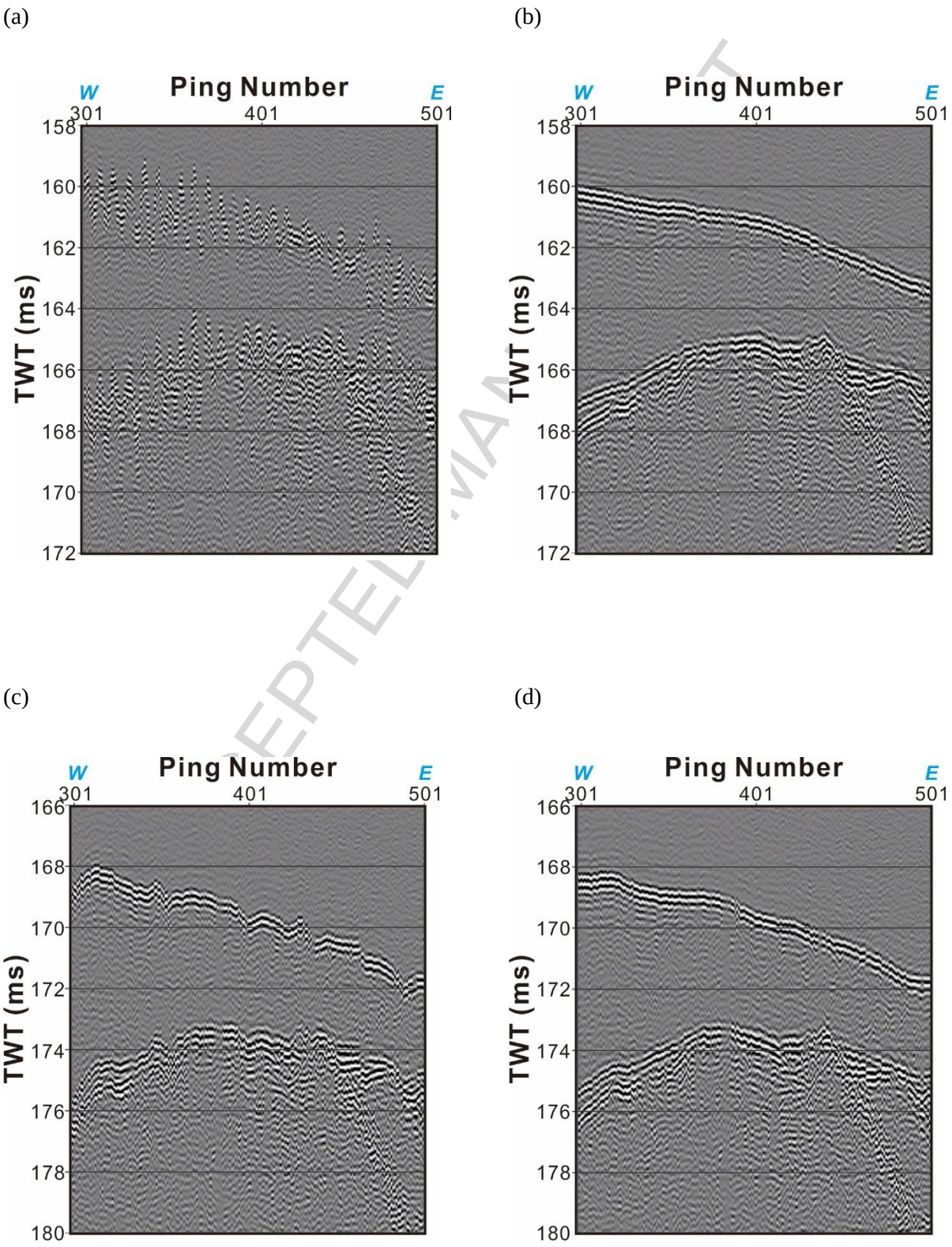

(e)

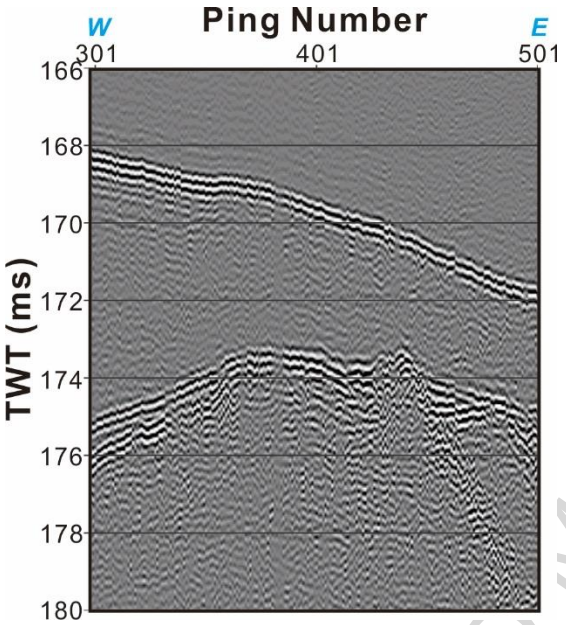

(f)

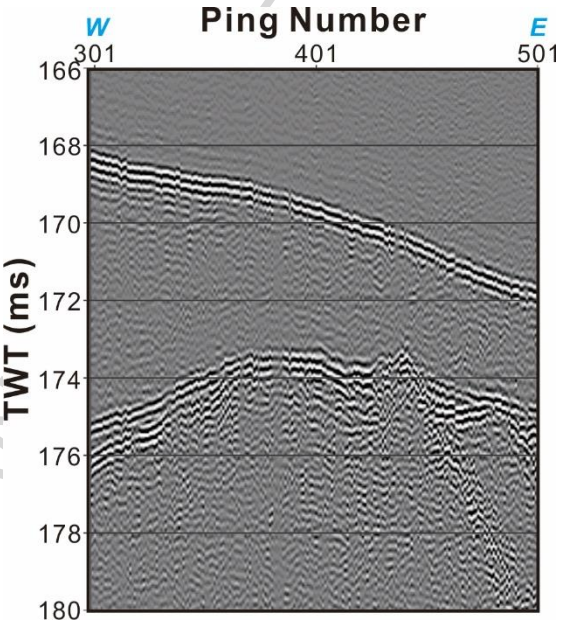

Figure 6.

(a)

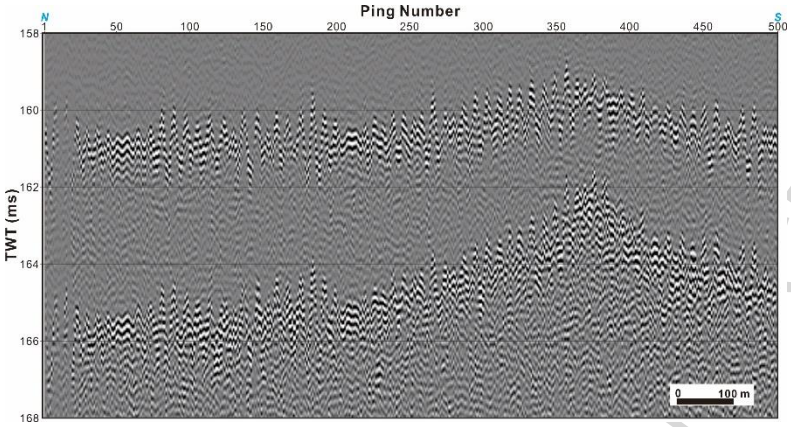

(b)

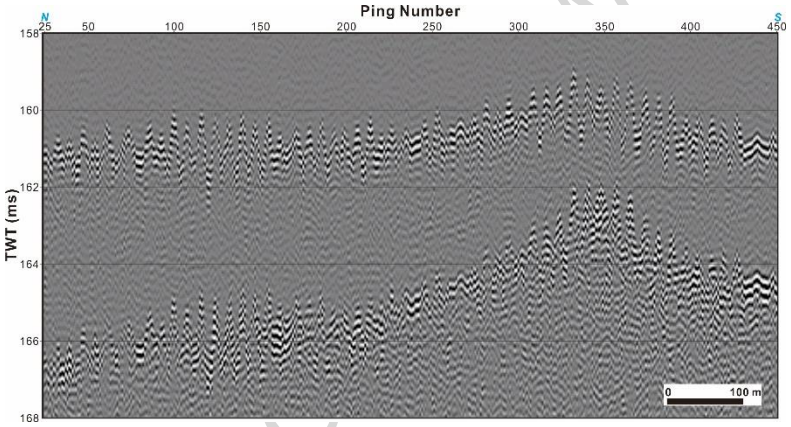

(c)

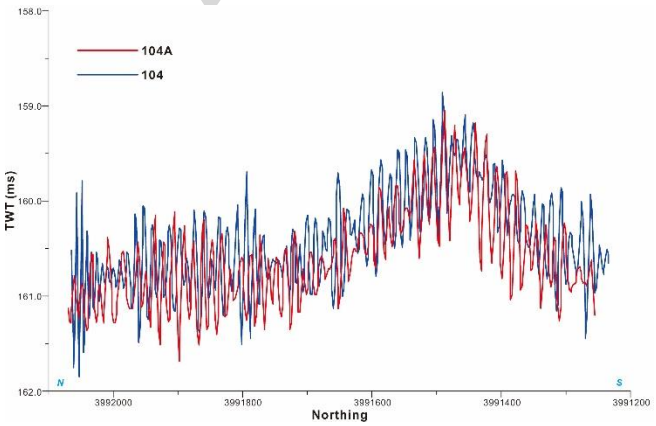

(d)

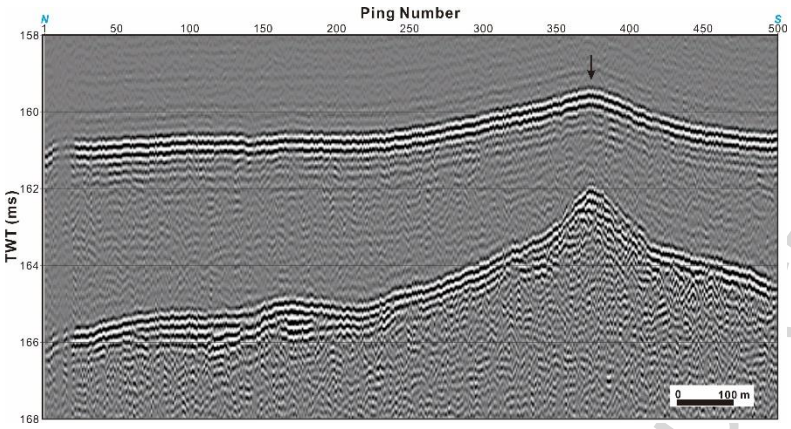

(e)

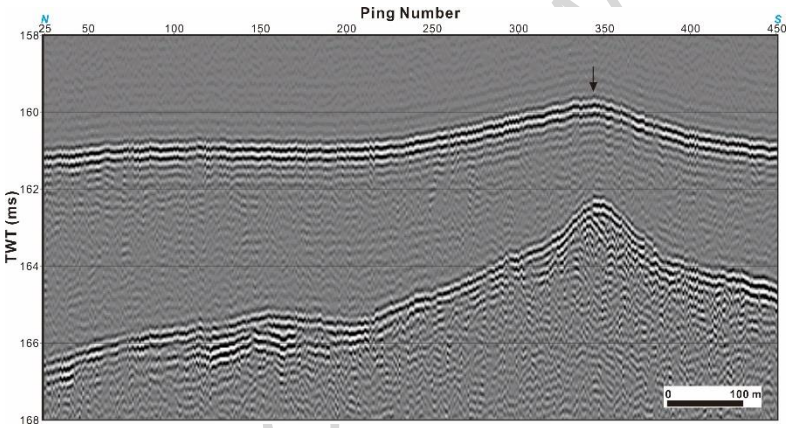

(f)

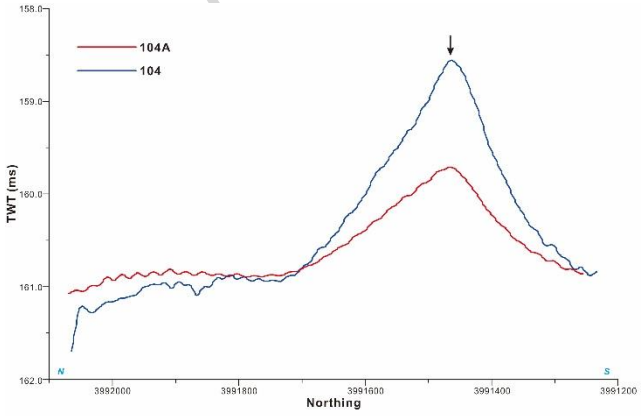

(g)

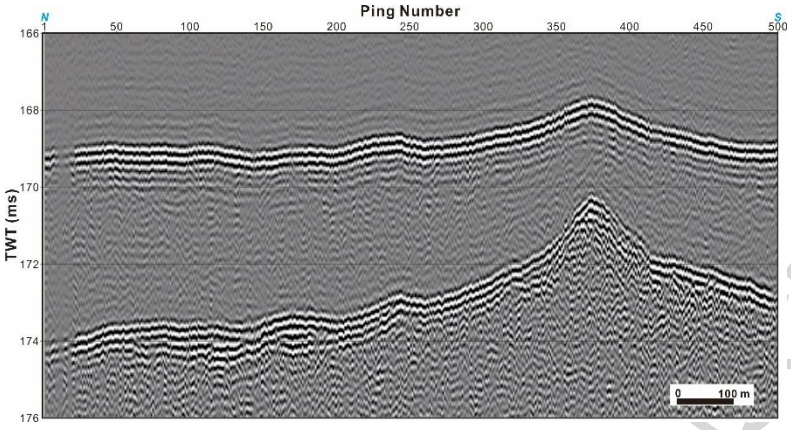

(h)

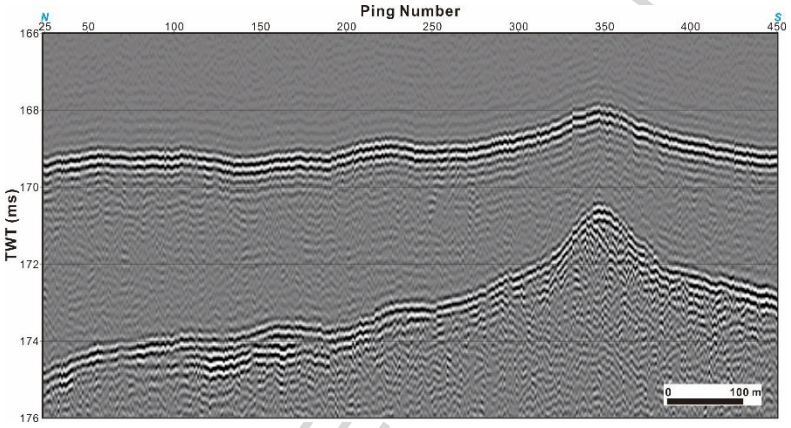

(i)

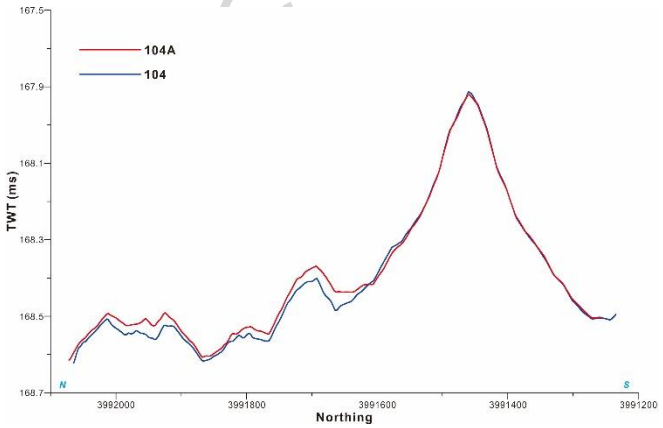

Figure 7.

(a)

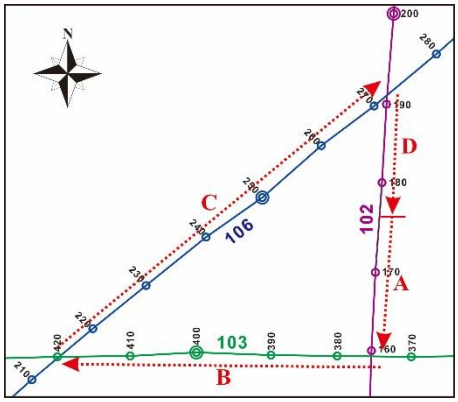

(b)

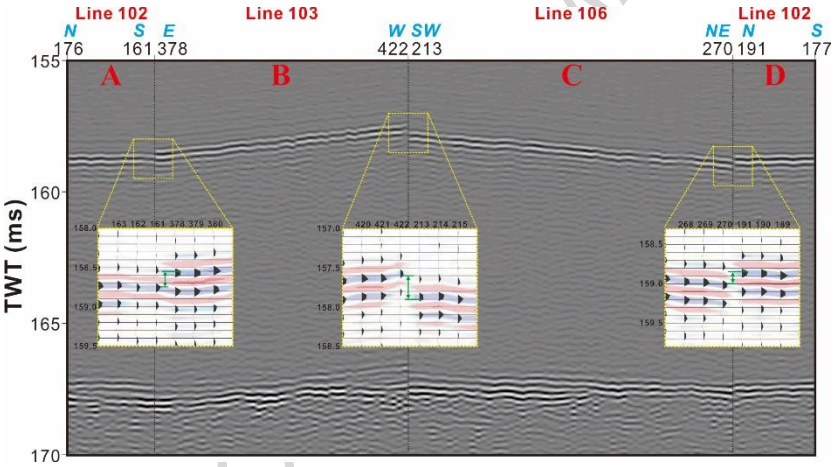

(c)